

The 10-rotation Periodicity in Sunspot Areas

R. Getko

© Springer ●●●

Abstract I study the sunspot area fluctuations over the epoch of 12 solar cycles (12-23). Lately, I found three significant quasi-periodicities at 10, 17 and 23 solar rotations, but two longer periods could be treated as subharmonics of the 10-rotation period. Thus, I search this period during the low- and the high-activity periods of each solar cycles. Because of the N-S asymmetry I consider each solar hemisphere separately. The skewness of each fluctuation probability distribution suggests that the positive and the negative fluctuations could be examined separately. To avoid the problem when a few strong fluctuations could create an auto-correlation or a wavelet peak, I also analyse the transformations of fluctuations for which the amplitudes at the high- and the low-activity periods are almost the same. The auto-correlation and the wavelet analyses show that the 10-rotation period is mainly detected during the high-activity periods, but it also exists during a few low-activity periods.

Keywords: Sunspots, Statistics; Solar Cycle, Observations

1. Introduction

In the last decades, the mid-term quasi-periodicities of many solar activity tracers have been discussed. Wolff (1983) reported the about 12 rotations periodicity in the monthly Wolf number variations from 1749 to 1979. This periodicity was also found in many solar activity indicators. Delarche, Laclare and Sadsoud (1987) detected it in the solar diameter measurements during cycle 21.

Lean and Brueckner (1989) found it in the power spectrum of the sunspot blocking function, 10.7 cm radio flux, sunspot number and plage index daily data during the three solar cycles (Nos. 19-21). Pap, Tobiska and Bouwer (1990) showed that an 8-11 month period existed in the total and UV irradiances (1980 and 1982-1988 respectively), 10.7 radio flux (1947-1989), the Ca K plage index (1970-1987), the sunspot blocking function (1874-1982) and the Mg II core-wing ratio (1978-1986). Akioka *et al.* (1987) detected it in areas and numbers of sunspot groups from 1969 to 1986. Oliver *et al.* (1992) studied daily sunspot numbers from 6 to 21 solar cycles. They adopted two different power spectrum methods and found a periodicity of about 323 days in three solar cycles only. They also

Astronomical Institute, University of Wrocław, Poland,
email: getko@astro.uni.wroc.pl

found a significant periodicity at 350 days (13 rotations) during cycles 12-21 together and in some individual cycles. Getko (2006) found statistically significant quasi-periodicity of about 9 months (10 rotations) in both high- and low-activity periods for the monthly Wolf number fluctuations from 1 to 22 solar cycles and for the group sunspot number fluctuations from 5 to 18 solar cycles.

Two longer periods at 17 rotations and at 23 rotations were found in many solar activity parameters. More up to date review is by Obridko and Shelting (2007). Lately, Getko (2009) showed that they could be treated as subharmonics of the 10-rotation period. This facts could explain a wide range of periodicities in various solar indices at all levels from the tachocline to the Earth.

In this paper, I search the 10-rotation period in the sunspot areas during the low- and the high-activity periods for cycles 12-23. The N-S asymmetry of solar activity (Vizoso and Ballester, 1990) suggests that both hemispheres should be considered separately. Because each empirical probability distribution of fluctuations is asymmetrical, the positive and the negative fluctuations are considered separately. To avoid the problem when a few strong fluctuations could create an auto-correlation or a wavelet peak, I transform each fluctuation time series into a new time series which has a constant variance (Getko, 2006). The amplitudes of each new time series at the high- and the low-activity periods are almost the same. The auto-correlation and the wavelet analyses of the original fluctuations and their transformations are used to find the mid-term periodicities from high- and low-activity periods in each solar cycle.

2. The Stationary Version of Sunspot Area Fluctuations

I consider the daily sunspot areas for the northern hemisphere (D_i^n), and the southern hemisphere (D_i^s) for solar cycles 12-23 available at the National Geophysical Data Center (NGDC)

(<http://solarscience.msfc.nasa.gov/greenwch/>). For the i -th Carrington rotation I evaluate the mean area for the northern hemisphere (S_i^n): $S_i^n = \frac{1}{K} \sum_{l=1}^K D_l^n$, where K is the number of days for the i -th rotation. I define the fluctuation (F_i^n) of the mean area (S_i^n) from the smoothed mean area: $F_i^n = S_i^n - \overline{S_i^n}$ for $i = 1, \dots, N$, where $\overline{S_i^n} = \frac{1}{13} \sum_{j=i-6}^{i+6} S_j^n$. Each of $\{F_i^n\}$ and $\{F_i^s\}$ contains $N = 1706$ elements. The beginning and the end of each cycles is defined by the minima of the smoothed monthly Wolf numbers. Each time series has the zero mean value and the time-dependent variance. To stabilize the variance I apply the procedure which is shown by Getko (2006) in Appendix. For the i -th rotation the value X_i^n of the new time series $\{X_i^n\}_{i=1}^N$ is a function of two parameters k and u (see equation (A2) in the Appendix). I estimate the values k and $\log A$ from equation (A10). The best solution is for $u = 13$ (rotations) and $k = 0.68 \pm 0.02$. For $\{F_i^s\}$ it is for $u = 13$ (rotations) and $k = 0.83 \pm 0.02$. Both the coefficients k are statistically significant (the F-statistic is used).

To verify the stationarity conditions of $\{X_i^n\}$ and $\{X_i^s\}$ the means ($\overline{X} = \frac{1}{u} \sum_{j=i_1 - [\frac{u}{2}]}^{i_1 + [\frac{u}{2}]} X_j$), standard deviations ($\overline{\sigma} = \sqrt{\frac{1}{u} \sum_{j=i_1 - [\frac{u}{2}]}^{i_1 + [\frac{u}{2}]} (X_j - \overline{X})^2}$), and auto-correlation functions (c_τ) are computed. For each time series about 70%

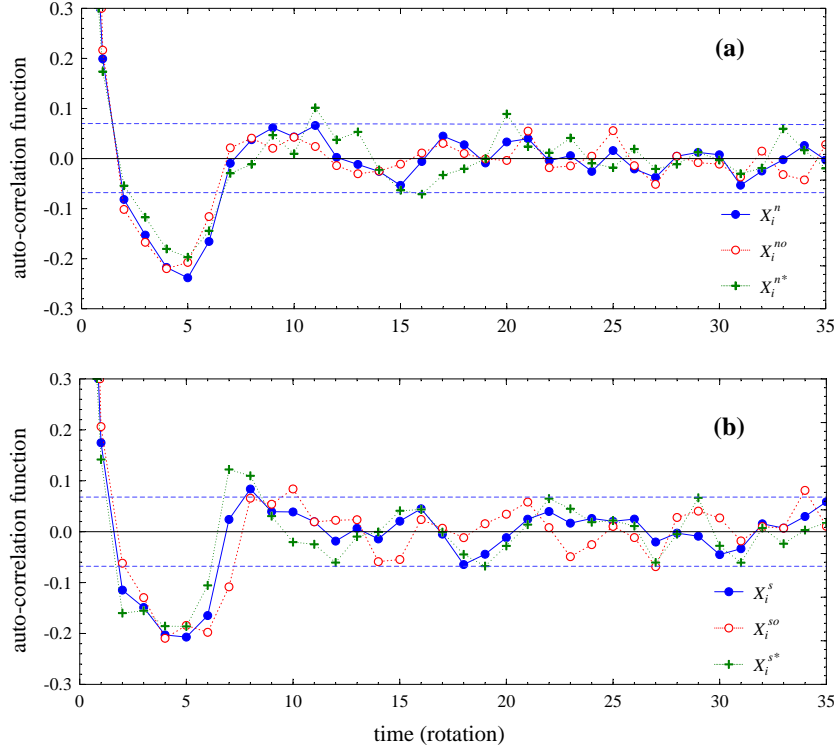


Figure 1. (a) Auto-correlation functions (c_τ) of $\{X_i^n\}$, $\{X_i^{no}\}$ and $\{X_i^{n*}\}$ (for all the data combined). The dashed horizontal lines represent two standard errors for each c_τ functions. (b) Same as for (a), but for $\{X_i^s\}$, $\{X_i^{so}\}$ and $\{X_i^{s*}\}$.

of the values of $\overline{\mathcal{X}}$ for $u = 13$ and $i_1 = 7, 20, \dots, 1698$ belong to the interval $(\overline{\mathcal{X}} - \hat{\sigma}, \overline{\mathcal{X}} + \hat{\sigma})$, where $\overline{\mathcal{X}}^n \approx -0.15$ and $\hat{\sigma}^n \approx 0.7$, and $\overline{\mathcal{X}}^s \approx -0.08$, and $\hat{\sigma}^s \approx 0.3$. All sample standard deviations for each time series belong to the interval $(\overline{\sigma} - 2\hat{\sigma}, \overline{\sigma} + 2\hat{\sigma})$, where $\overline{\sigma}^n \approx 4.4$ and $\hat{\sigma}^n \approx 0.4$ and $\overline{\sigma}^s \approx 1.8$ and $\hat{\sigma}^s \approx 0.2$. Figs. 1a and 1b show the c_τ functions of $\{X_i\}$, $\{X_i^o\}$ and $\{X_i^*\}$ for all 12 cycles for the northern and the southern hemispheres respectively. Here $\{X_i^o\}$ and $\{X_i^*\}$ are computed after dividing $\{X_i\}_{i=1}^N$ into two parts: those from the periods of high and low sunspot activities, respectively. To evaluate these periods the smoothed monthly Wolf numbers $\{\overline{R}_m\}_{m=1}^{N_1}$ are used. All m for which the values \overline{R}_m are less (greater) than the mean value of $\{\overline{R}_m\}$ define low (high) activity periods. Two standard errors for each c_τ are plotted as the dashed horizontal lines. Because each of three time series has a different length M , the bounds for the shortest time series are plotted (± 0.068). The differences between the c_τ functions of $\{X_i^{no}\}$ and $\{X_i^{n*}\}$ are greater than 2σ for $\tau = 11, 13, 16, 17, 20, 25, 33, 34$ rotations. For the southern hemisphere both the c_τ functions significantly differ at $\tau = 7, 10, 12, 15, 19, 23, 30, 34$ rotations. Although the means and the standard deviations of $\{X_i\}$, $\{X_i^o\}$ and $\{X_i^*\}$ are

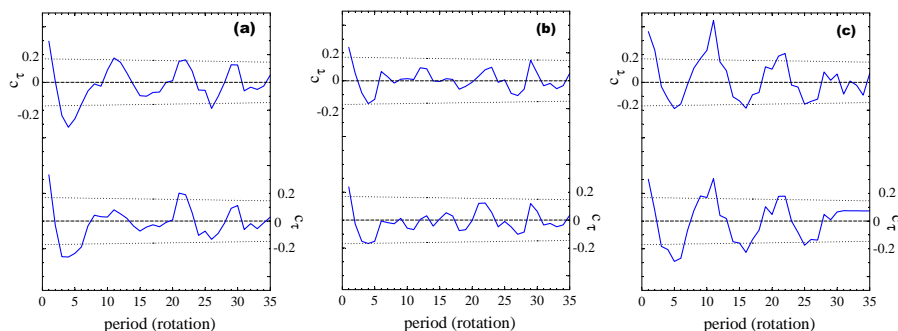


Figure 2. (a) *Top*: Auto-correlation function (c_τ) of $\{F_i^n\}$ for cycle 18. *Bottom* Same as for the upper curve, but for $\{X_i^n\}$. The dotted lines represent two standard errors of each c_τ function. (b) The same as for (a), but for $\{F_i^{n+}\}$ and $\{X_i^{n+}\}$. (c) The same as for (a), but for $\{F_i^{n-}\}$ and $\{X_i^{n-}\}$.

approximately constant the c_τ functions are different. Thus, $\{X_i^n\}$ and $\{X_i^s\}$ are not stationary.

Because each fluctuation probability distribution has positive skew (Getko, 2009), the positive and the negative fluctuations are considered separately. For $\{F_i^n\}$ they can be defined as follows:

$$F_i^{n+} = \begin{cases} 0 & \text{where } F_i^n \leq 0 \\ F_i^n & \text{where } F_i^n > 0 \end{cases} \quad \text{for } i = 1, \dots, N.$$

$$F_i^{n-} = \begin{cases} 0 & \text{where } F_i^n > 0 \\ F_i^n & \text{where } F_i^n \leq 0 \end{cases} \quad \text{for } i = 1, \dots, N.$$

The same definitions are applied to X_i^{n+} and X_i^{n-} , and to all these time series for the southern hemisphere.

3. The periodicities during high- and low-activity periods

To find the periodicities during high-activity periods I apply the auto-correlation function (c_τ). The original, the positive and the negative fluctuations are considered separately. The same is for transformations. I divide each of them into 12 parts of length $L \approx 11$ years. For example, for the northern hemisphere I consider $\{F_i^n\}_{i=1}^L$, $\{X_i^n\}_{i=1}^L$, $\{F_i^{n+}\}_{i=1}^L$, $\{X_i^{n+}\}_{i=1}^L$, $\{F_i^{n-}\}_{i=1}^L$ and $\{X_i^{n-}\}_{i=1}^L$ for each of 12 cycles. Figs. 2a-c show their functions c_τ for cycle 18. For the c_τ of $\{F_i^n\}$ (Fig. 2a, top) a global maximum is greater than 2σ at $\tau = 11$ rotations, for $\{X_i^n\}$ (bottom) the value c_{11} is less than 1σ . Moreover, for $\{F_i^{n+}\}$ the value c_{12} is between 1σ and 2σ and for $\{X_i^{n+}\}$ it is less than 1σ (Fig. 2b). A decrease of c_τ at $\tau \in [7, 13]$ rotations, which is at least 1σ , is in 71% of 24 cases (12 cycles in each hemisphere). Because the transformation of $\{F_i^n\}$ into $\{X_i^n\}$ stabilizes the variance of $\{F_i^n\}$ such a decrease is probably created by strong fluctuations from the high-activity period. Moreover, the width of the c_τ maximum of $\{F_i^{n+}\}$

(evaluated for the 1σ level) is between two and five rotations. There are also a few cases (for example, for $\{F_i^{s+}\}$ cycles 13, 14, 18, 19, 20) for which each function c_τ has two or three peaks (their width for the 1σ level is one rotation). This means, that the strong fluctuations are quasi-periodical. Fig. 2c shows that for $\{F_i^{n-}\}$ and $\{X_i^{n-}\}$ in cycle 18 both c_{11} are greater than 2σ . This could indicate that the fluctuations from the whole cycle create both peaks. In addition, a decrease of c_{11} (it is at least 1σ) could be created by fluctuations from the high-activity period. It is also found in 80% of 24 cases. The longer c_τ periods are treated as subharmonics of about 10-rotation period (Getko, 2009).

I also apply the Morlet wavelet (Torrence and Compo, 1998) to six time series for each of 24 cases. Fig. 3a (top) shows the local spectrum of $\{F_i^n\}$ for cycle 18. Black solid contours denote the 95 per cent significance level for detected peaks. The global maximum of the integrated spectrum (right) at $\tau = 11$ rotations is mainly created by fluctuations from the high-activity period. It confirms the auto-correlation result (Fig. 1a). Similar wavelet map is for $\{F_i^{n+}\}$ (bottom), but the peak at $\tau = 11$ rotations is significant. The global spectrum shows two almost the same peaks at $\tau = 11$ and 8 rotations. The wavelet map of $\{X_i^n\}$ (Fig. 3b, top) for the high-activity period is almost the same as for $\{F_i^n\}$. The global spectrum for $\{X_i^{n+}\}$ is also almost the same as for $\{F_i^{n+}\}$, but the wavelet power at $\tau = 11$ rotations is significant for $\{F_i^{n+}\}$ while for $\{X_i^{n+}\}$ it is not significant. For $\{F_i^{n-}\}$ and $\{X_i^{n-}\}$ in each wavelet map the strongest peak at $\tau = 11$ rotations is significant (Figs. 3a and 3b, middle). It extends in time during the high-activity period and dominates the integrated spectrum. Moreover, the wavelet map of $\{X_i^{n-}\}$ shows this periodicity during the declining portion of cycle 18 and smaller power at $\tau \approx 8$ rotations during the rising portion of cycle 18. The same was done for all 24 cases. The wavelet and the auto-correlation results are similar for $\tau \in [7, 13]$ rotations (the correlation between them is about 0.9 for 87%, 72%, 92%, 61% and 75% of the c_τ peaks of $\{F_i^n\}$, $\{F_i^{n+}\}$, $\{F_i^{n-}\}$, $\{X_i^n\}$ and $\{X_i^{n+}\}$ respectively). For $\{X_i^-\}$ the correlation is about 0.8 for 83% of c_τ peaks.

To find the periodicities during the low-activity periods I examine the wavelets for 12 cycles together. The map of $\{X_i^{n+}\}$ shows the significant peaks at about 10 rotations from these periods (cycles 13-14, 15-16, 17-18, 20-21). For $\{X_i^{n-}\}$ there are also several significant peaks (cycles 13-14, 16-17, 17-18, 18-19 and 20-21). Both maps of $\{X_i^{s+}\}$ and $\{X_i^{s-}\}$ also show significant peaks during these periods (cycles 12-13, 13-14, 15-16, 16-17, 18-19 and cycles 12-13, 15-16, 16-17 respectively).

4. Discussion

The transformation of fluctuations into the new time series with a constant variance enables one to evaluate the time intervals where the functions c_τ have the most dominant periods. Such analyses indicate that the mean time distance between strong fluctuations from solar maxima is about 10 rotations for each hemisphere separately. Moreover, the division of $\{X_i\}$ for each hemisphere into two shorter parts: containing data from low-activity periods ($\{X_i^*\}$) and from

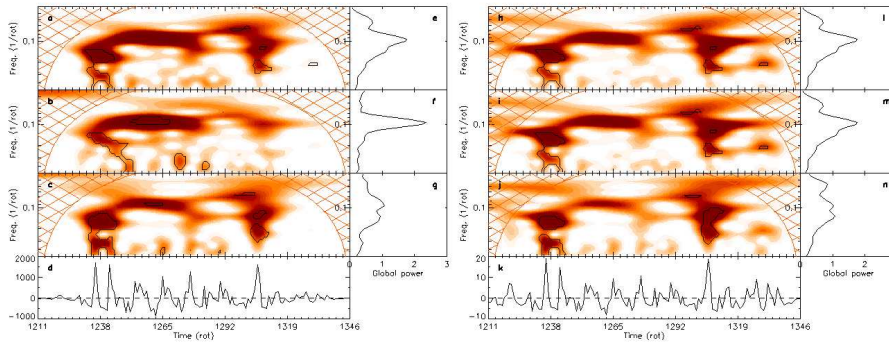


Figure 3. **a-c:** Wavelet power spectra of **a:** $\{F_i^n\}$, **b:** $\{F_i^{n-}\}$ and **c:** $\{F_i^{n+}\}$ mapping a time-frequency evolution of about 10-rotation periodicity. Top values of wavelet power are denoted by gradual darkening. Black contours denote significance levels of 95 per cent for detected peaks. A cone of influence is marked by the dashed region. **e-g:** Corresponding global wavelet power spectra. **d:** Time series $\{F_i^n\}$ for cycle 18. **h-n:** Same as **a-g**, but $\{X_i^n\}$, $\{X_i^{n-}\}$ and $\{X_i^{n+}\}$.

high-activity periods ($\{X_i^o\}$) enables one to verify possible differences between periodicities existing during these periods in 12 solar cycles.

For each hemisphere the functions c_τ of all three these time series have wide global maxima at $\tau \in [7, 13]$ rotations. The functions c_τ of $\{X_i^n\}$ and $\{X_i^{n*}\}$ have the significant global maxima at $\tau = 11$ rotations, but for $\{X_i^{no}\}$ two local maxima at 8 and 10 rotations are between 1σ and 2σ . For the southern hemisphere all three global maxima are greater than 2σ . For $\{X_i^{so}\}$ this maximum contains two almost the same peaks at $\tau = 8, 10$ rotations. These results confirm the wavelets for all time series. All global spectra have the dominant peaks at $\tau = 10$ rotations. For $\{X_i^{n+}\}$ and $\{X_i^{s+}\}$ these peaks are much wider and lower than for $\{X_i^{n-}\}$ and $\{X_i^{s-}\}$. These wide maxima indicate that the time separations between fluctuation maxima oscillate around the average length τ . This fact could be caused by the differential rotation and the different rotation rate of activity complexes during their life time (?). In addition, Getko (2004) shows that strong positive fluctuations are always created by 2-4 activity complexes which have not their largest size at the same time (the maxima of their contribution to the monthly Wolf number are shifted from one to three months). Namely, the fluctuations are not strictly periodical, but quasi-periodical. Moreover, because the functions c_τ (and the wavelets) of positive and of negative fluctuations are different, the positive fluctuations, which describe a strong magnetic flux emergence, are rather a sequence of pulses following at fixed time intervals than harmonic oscillations (Obridko and Shelting, 2007). In addition, for $\{F_i^{n+}\}$ and $\{F_i^{s+}\}$ the significant wavelet peaks at 10 rotations usually exist during short time intervals of high-activity periods and also exist in the maps of $\{X_i^{n+}\}$ and $\{X_i^{s+}\}$ during several low-activity periods.

I also obtained similar results for the monthly Wolf numbers and for the group sunspot numbers during high-activity periods (Getko, 2006). For periods around 11-12 rotations Prabhakaran Nayar *et al.* (2002) showed a significant wavelet power of the daily Wolf numbers for short time intervals during several

solar maxima. Taking into consideration that the solar activity fluctuations are quasi-periodical, the results obtained for daily data and data used in this paper are similar. Moreover, an analysis of the auto-correlation of daily sunspot areas for solar cycles 10-20 (Bogart, 1982) leads to the evidence for the existence of a few sites of unusually strong solar activity in each solar cycle that persist for about 10 rotations and generally rotate with a period of about 27 days.

5. Conclusions

The following results have been obtained:

1. The auto-correlation and the wavelet analyses of the original, the positive and the negative fluctuations and their transformations prefer the 10-rotation quasi-periodicity.
2. The differences between the auto-correlation maxima (for $\tau \in [7, 13]$ rotations) of fluctuations and their transformations suggest that the 10-rotation period is created by strong fluctuations from high-activity periods.
3. The wavelet analysis confirms auto-correlation results for $\tau \in [7, 13]$ rotations (the correlation is about 0.9 for 87%, 72%, 92%, 61% and 75% of the auto-correlation peaks of $\{F_i^n\}$, $\{F_i^{n+}\}$, $\{F_i^{n-}\}$, $\{X_i^n\}$ and $\{X_i^{n+}\}$ respectively, and it is 0.8 for 83% of the auto-correlation peaks of $\{X_i^{n-}\}$).
4. The wavelet maps of $\{X_i^{n+}\}$, $\{X_i^{n-}\}$, $\{X_i^{s+}\}$ and $\{X_i^{s-}\}$ for all 12 solar cycles together show several statistically significant peaks at about 10 rotations for low-activity periods. This means that during these periods small quasi-periodical fluctuations exist.

References

- Akioka, M., Kubota, J., Suzuki, M., Ichimoto, K., and Tohmura, I.: 1987, *Solar Phys.* **112**, 313.
- Bogart, R. S.: 1982, *Solar Phys.* **76**, 155.
- Brockwell, P. J. and Davis, R. A.: 1991, *Time Series: Theory and Methods*, Springer, New York.
- Delache, P., Laclare, F., and Sadsoud, H.: 1985, *Nature* **317**, 416.
- Gaizauskas, V., Harvey, K.L., Harvey, J.W., and Zwaan, C.: 1983, *Astrophys. J.* **265**, 1056.
- Getko, R.: 2004, newblock *Solar Phys.* **224**, 291.
- Getko, R.: 2006, *Solar Phys.* **238**, 187.
- Getko, R.: 2009, The Mid-term Periodicities in Sunspot Areas., in: *Proceedings of IAU 257 Symposium, Universal Heliophysical Processes*, Cambridge University Press, pp. 169-172.
- Lean, J.L. and Brueckner, G.E.: 1989, *Astrophys. J.* **337**, 568.
- Obridko, V.N., Shelting, B.D.: 2007, *Adv. Space Res.* **40**, 1006.
- Oliver, R., Carbonell, M., Ballester, J.L.: 1992, *Solar Phys.* **137**, 141.
- Pap, J., Tobiska, W.K., and Bouwer, S.D.: 1990, *Solar Phys.* **129**, 165.
- Prabhakaran Nayar, S. R., Radhida, V. N., Revathy, K., and Ramadas, V.: 2002, *Solar Phys.* **208**, 359.
- Torrence, C., Compo, G.P.: 1998, *Bul. Am. Meteor. Soc.* **79**, 61.
- Vizoso, G., Ballester, J. L.: 1990, *Astron. Astrophys.* **229**, 540.
- Wolff, C.L.: 1983, *Astrophys. J.* **264**, 667.

